

Northumbria Research Link

Citation: Wang, Qian, Kalathil, Shafeer, Pornrungrroj, Chanon, Sahm, Constantin D. and Reisner, Erwin (2022) Bacteria-photocatalyst sheet for sustainable carbon dioxide utilization. *Nature Catalysis*, 5 (7). pp. 633-641. ISSN 2520-115

Published by: Springer Nature

URL: <https://doi.org/10.1038/s41929-022-00817-z> <<https://doi.org/10.1038/s41929-022-00817-z>>

This version was downloaded from Northumbria Research Link:
<https://nrl.northumbria.ac.uk/id/eprint/50138/>

Northumbria University has developed Northumbria Research Link (NRL) to enable users to access the University's research output. Copyright © and moral rights for items on NRL are retained by the individual author(s) and/or other copyright owners. Single copies of full items can be reproduced, displayed or performed, and given to third parties in any format or medium for personal research or study, educational, or not-for-profit purposes without prior permission or charge, provided the authors, title and full bibliographic details are given, as well as a hyperlink and/or URL to the original metadata page. The content must not be changed in any way. Full items must not be sold commercially in any format or medium without formal permission of the copyright holder. The full policy is available online: <http://nrl.northumbria.ac.uk/policies.html>

This document may differ from the final, published version of the research and has been made available online in accordance with publisher policies. To read and/or cite from the published version of the research, please visit the publisher's website (a subscription may be required.)

Bacteria-photocatalyst sheet for sustainable carbon capture and utilisation

Qian WANG,^{1,†} Shafeer KALATHIL,^{1,2,†} Chanon PORNRUNGROJ,¹ Constantin D. SAHM,¹ Erwin REISNER^{1,*}

Affiliation and full postal address

1 *Yusuf Hamied Department of Chemistry, University of Cambridge, Lensfield Road, Cambridge CB2 1EW, UK*

2 *Hub for Biotechnology in the Built Environment, Department of Applied Sciences, Faculty of Health and Life Sciences, Northumbria University, Newcastle upon Tyne, NE1 8ST, UK*

† Equal contribution

***Corresponding author**

Professor Erwin REISNER

Yusuf Hamied Department of Chemistry, University of Cambridge, Lensfield Road, Cambridge CB2 1EW, UK

Tel: +44-1223336323

E-mail: reisner@ch.cam.ac.uk

Abstract

The clean conversion of carbon dioxide and water to a single multicarbon product and O₂ using sunlight via photocatalysis without the assistance of organic additives or electricity remains an unresolved challenge. Here we report a bio-abiotic hybrid system with the nonphotosynthetic, CO₂-fixing acetogenic bacterium, *Sporomusa ovata* (*S. ovata*) grown on a scalable and cost-effective photocatalyst sheet consisting of a pair of particulate semiconductors (La and Rh co-doped SrTiO₃ (SrTiO₃:La,Rh) and Mo-doped BiVO₄ (BiVO₄:Mo)). The biohybrid effectively produces acetate (CH₃COO⁻) and oxygen (O₂) using only sunlight, CO₂ and H₂O, achieving a solar-to-acetate conversion efficiency of 0.7%. The photocatalyst sheet oxidises water to O₂ and provides electrons and hydrogen (H₂) to *S. ovata* for the selective synthesis of CH₃COO⁻ from CO₂. To demonstrate the utility in a closed carbon cycle, the solar-generated acetate was used directly as feedstock in a bioelectrochemical system for electricity generation. These semi-biological systems thus offer a promising strategy for sustainably and cleanly fixing CO₂ and closing the carbon cycle.

Artificial photosynthesis aims to convert H₂O and CO₂ with intermittent solar energy into storable fuels. The sunlight-driven CO₂ reduction reaction (CO₂RR) to form multicarbon products (C_{2/2+}) using inorganic catalysts is challenging because they typically provide poor selectivity toward C_{2/2+} products and necessitate additional electricity input to offset the large overpotential requirements.¹⁻⁶ In contrast, nonphotosynthetic, CO₂-fixing bacteria have metabolic pathways that can produce C_{2/2+} from CO₂ with high selectivity and display relatively high stability toward environmental perturbations.⁷⁻¹¹ Thus, hybrid bio-abiotic systems consisting of synthetic light absorbers assembled with CO₂-fixing bacteria provide the opportunity for solar-powered CO₂-to-C_{2/2+} conversion, which harnesses the efficient light-harvesting capabilities of semiconductors and the strong catalytic power of living biocatalysts.^{9,12}

Among several prototypes of such hybrid bio-abiotic systems for photosynthetic CO₂ fixation, photovoltaic-driven electrolysis or photoelectrochemical (PEC) cells are under development.¹³⁻¹⁷ These approaches either rely on large quantities of an intermediate fuel such as H₂ or syngas being generated to feed the bacteria in a separate compartment or suffer from local pH gradients and IR drops (a potential drop due to solution resistance) occurring during the redox reactions in a close to neutral pH solution when directly integrated into (photo)electrodes.^{18,19} Additionally, the preparation of solar cells and (photo)electrodes is typically complex, often requiring vacuum processes.^{14,15,20-22}

A more straightforward route to establish bio-abiotic hybrids is to apply a colloidal system that uses particulate photocatalysts attributable to their simpler design and potentially lower cost.²²⁻²⁴ However, colloidal biohybrid systems require commonly the addition of sacrificial reagents,²⁵⁻²⁷ as the photosensitizer is usually unable to catalyze water oxidation. Cysteine has been widely used as a sacrificial electron donor to quench the photogenerated holes, exemplified by the CO₂-to-acetate reducing photobiohybrid of *Moorella thermoacetica*|CdS (*M. thermoacetica*|CdS).²⁶ However, a recent study showed acetate production in this biohybrid system even in the absence of light and

demonstrated a cysteine-dependent metabolic pathway for acetate production.²⁸ Cysteine is also a known electron mediator for microbial respiration,^{29,30} and functioned as an electron donor in iron reduction by *Shewanella* species.³⁰ Thus, sacrificial reagents and organic additives should be avoided in the development of photobiohybrid systems to achieve sustainable and clean CO₂ conversion.

Constructing Z-scheme systems using two complementary light harvesters for photoreduction and photooxidation, respectively, provides a platform to drive CO₂RR and water oxidation simultaneously without sacrificial reagents or organic mediators.³¹ However, Z-scheme systems using bio-abiotic hybrids remain scarce because of the difficulty to establish efficient interparticle electron transfer between the light absorbers. An attempt has been made to combine *M. thermoacetica*|CdS with a TiO₂ nanoparticle loaded with a manganese(II) phthalocyanine, using a cysteine/cystine redox couple as the electron relay.¹⁷ This tandem system has been reported to produce acetate and O₂ simultaneously, but the efficiency and stability are limited due to side reactions caused by the redox couple.

Monolithic photocatalyst sheets contain an immobilised pair of semiconductor nanoparticles with narrow bandgaps (e.g. SrTiO₃:La,Rh and BiVO₄:Mo) on a conductive inorganic layer (e.g. gold and carbon).^{19,32} These photocatalyst sheets can achieve unassisted, scalable, and efficient light-driven water splitting and CO₂-to-formate conversion as the interparticle electron transfer is facilitated by solid conductive mediators. Furthermore, the reduction and oxidation reactions occur in close vicinity in the photocatalyst sheets, which can largely suppress the local pH changes during the redox reactions.³² The photocatalyst sheets display pH-independent (pH 2.5-7.5) activity and therefore achieve overall water splitting without adjusting the pH or adding buffer.³³ The photocatalyst sheet design is thus expected to overcome the hurdles commonly observed in (photo)electrochemical and conventional photocatalytic colloidal systems and is a particularly

promising platform for the assembly of hybrid bio-abiotic systems due to the high solar-to-fuel conversion efficiency operating at a biocompatible neutral pH.

Here we report that a photocatalyst sheet ($\text{Cr}_2\text{O}_3/\text{Ru-SrTiO}_3:\text{La,Rh}|\text{ITO}|\text{RuO}_2\text{-BiVO}_4:\text{Mo}$), which is prepared by a relatively inexpensive and readily accessible drop-casting method, combined with CO_2 -fixing acetogenic bacteria (*S. ovata*) results in selective CH_3COO^- production coupled to O_2 evolution using only sunlight, CO_2 , and H_2O , with a solar-to-acetate conversion efficiency (STA) of $0.70 \pm 0.04\%$. The electrons and protons for the CO_2RR must be sourced from H_2O without the consumption of sacrificial reagents in order to develop a sustainable process. However, reports of photocatalytic CO_2RR conjugated to water oxidation remain scarce.³⁴ This system does not require the addition of organics as a sacrificial reagent or redox couples, thereby demonstrating clean CO_2 -to-multicarbon conversion using hybrid biocatalysis at benchmark efficiency.

Results

Assembly of the biohybrid system

S. ovata was selected as a microbe because it can efficiently catalyse the CO_2RR to CH_3COO^- by using H_2 or electrons directly from an electrode in microbial electrosynthesis.^{14,35} $\text{SrTiO}_3:\text{La,Rh}$ and $\text{BiVO}_4:\text{Mo}$ nanoparticles were chosen as light harvesters in the Z-scheme photocatalysts (Figure 1a and Supplementary Fig.1), because they can absorb visible light, with an absorption edge of 520 nm (Supplementary Fig.2).^{19,36} Indium tin oxide (ITO) nanoparticles (Supplementary Fig.1) act as charge mediators to connect $\text{SrTiO}_3:\text{La,Rh}$ and $\text{BiVO}_4:\text{Mo}$ particles and display high transparency to visible light without catalysing side-reactions (i.e. O_2 reduction reaction).^{37,38}

The $\text{SrTiO}_3:\text{La,Rh}|\text{ITO}|\text{BiVO}_4:\text{Mo}$ sheet (Figure 1b and Supplementary Fig. 3 and 4) was prepared by readily accessible and scalable drop-casting (see Methods). The $\text{Cr}_2\text{O}_3/\text{Ru}$ and RuO_2 were subsequently loaded on the $\text{SrTiO}_3:\text{La,Rh}$ and $\text{BiVO}_4:\text{Mo}$ by photodeposition, respectively, to

construct the H₂ evolution photocatalyst (Cr₂O₃/Ru-SrTiO₃:La,Rh) and the O₂ evolution photocatalyst (RuO₂-BiVO₄:Mo) (Figure 1a). The Ru and RuO₂ nanoparticles provide active sites for H₂ and O₂ evolution, respectively, whereas the Cr₂O₃ shell prevents access of O₂ molecules to the Ru surface and thereby suppresses the occurrence of the competitive O₂ reduction reaction.^{19,39} The loading amounts of Ru and Cr were estimated via inductively coupled plasma–optical emission spectrometry (ICP–OES) to be ~68 and ~20 nmol cm⁻² (geometrical surface area of sheet), respectively (Supplementary Table 1).

Scanning electron microscopy and energy dispersive X-ray spectroscopy (SEM–EDX) mapping images of the photocatalyst sheet (Supplementary Fig. 3 and 4) revealed the formation of a particle layer containing the SrTiO₃:La,Rh, BiVO₄:Mo, and ITO with a thickness of ~10 μm. The ITO nanoparticles aggregated to form large clusters, connecting the SrTiO₃:La,Rh and BiVO₄:Mo and providing pathways for interparticle electron transfer.^{37,38} The stacked particle layer with interparticle voids (several micrometres in diameter) is expected to provide easy access for bacterial colonization.⁴⁰

The *S. ovata*|sheet hybrid was assembled by immersing the Cr₂O₃/Ru-SrTiO₃:La,Rh|ITO|RuO₂-BiVO₄:Mo sheet (Supplementary Fig. 5 and 6) in an *S. ovata* medium (Supplementary Table 2). The sheet split water into H₂ and O₂ under light irradiation and acted as the sole electron and/or H₂ donor for the bacteria metabolism, leading to the growth of *S. ovata* onto the sheet during the photosynthetic reaction.

Photosynthetic activity

The water-splitting ability of the Cr₂O₃/Ru-SrTiO₃:La,Rh|ITO|RuO₂-BiVO₄:Mo sheet (~2.2 cm²) in the *S. ovata* medium (without the bacterium) purged with N₂ (pH 6.9) was confirmed under simulated solar irradiation (Air Mass 1.5 Global (AM 1.5G) filter, 100 mW cm⁻²). The sheet split

water into H₂ and O₂ in a stoichiometric ratio with a solar-to-hydrogen conversion efficiency of 0.62 ± 0.04% without forming any CO₂RR products (Supplementary Fig. 7 and Supplementary Table 3 and 4).

The CO₂RR was subsequently performed by using the same reaction medium purged with 80%N₂/20%CO₂ (pH 7.0) containing *S. ovata* cells (final optical density at 600 nm: 0.6). The biohybrid system produced CH₃COO⁻ (~ 9 mM) and O₂ simultaneously in the expected 1:2 ratio (Figure 2a) under 1 sun illumination, demonstrating closed redox cycle catalysis and ruling out that the presence of impurities functioned as sacrificial reductant/oxidant. Proton nuclear magnetic resonance (¹H NMR) spectroscopy (Supplementary Fig. 8) and gas chromatography confirmed that CH₃COO⁻ is the only detectable product of CO₂RR, with a small amount of H₂ also being detected (4.6 ± 0.9 μmol cm⁻² in 15 h). Accordingly, the selectivity for CH₃COO⁻ formation in the reduction reactions is ~90 % (~100% in CO₂RR). The photograph and SEM-EDX mapping images of the sample after the reaction (Figure 1c and 3 and Supplementary Fig. 1) revealed the presence of all components, including the *S. ovata* cells, on the photocatalyst sheet. Additionally, the concentrations of protein in the medium before the reaction and on the sheet (~2.2 cm²) after the reaction were estimated as 1.55 ± 0.18 and 0.59 ± 0.03 mg, respectively, further supporting that part of the *S. ovata* cells grow on the photocatalyst sheet surface during the photosynthetic reaction.

The formation of CH₃COO⁻ was observed for λ ≤ 510 nm irradiation (Figure 2c), consistent with the absorption onsets of both SrTiO₃:La,Rh and BiVO₄:Mo. An STA of 0.70 ± 0.04% was obtained and the apparent quantum yield (AQY) was 21.3% at 420 ± 15 nm. The AQY decreased with increasing wavelength of incident photons up to 510 nm, which is in reasonably good agreement with the diffuse reflectance spectra observed for SrTiO₃:La,Rh and BiVO₄:Mo. These results support an efficient Z-scheme mechanism derived by the photoexcited electron-hole pairs in the SrTiO₃:La,Rh and BiVO₄:Mo. The STA is higher than that of a tandem PEC cell composed of silicon nanowires as

the photocathode and titanium dioxide nanowires as the photoanode (0.38%).¹⁴ The pH gradient and IR drop during the redox reaction on the photocatalyst sheet are also largely suppressed and the presented system does therefore not require a strong electrolyte and buffer as required in classical PEC cells.³² In comparison to PEC cells, the preparation of photocatalyst sheet-bacteria hybrid is also less complicated and does not require vacuum processes, making it a relatively cost-effective process and provides the basis to scale-up the photosynthetic activity.

Isotopic labelling experiments showed that $^{13}\text{CO}_2/\text{H}^{13}\text{CO}_3^-$ was the sole carbon source for CH_3COO^- production (Figure 2d and Supplementary Fig. 9). ^1H NMR spectroscopy (Figure 2d) exhibited a doublet attributable to the ^{13}C -coupled proton with $^1J_{\text{CH}} = 127$ Hz and $^2J_{\text{CH}} = 6$ Hz, which is consistent with previous reports⁴¹ and the spectrum for an authentic sample of $^{13}\text{CH}_3^{13}\text{COONa}$ (Supplementary Fig. 10). The amount of $^{13}\text{CH}_3^{13}\text{COO}^-$ was decreased by half compared to $^{12}\text{CO}_2/\text{H}^{12}\text{CO}_3^-$ conditions (Supplementary Table 4), a phenomenon previously assigned to the propagation of isotopes through metabolic networks and their affected operation by kinetic isotope effects.^{42,43}

No products were detected in a series of deletional control experiments in which light, $\text{SrTiO}_3:\text{La,Rh}$, and $\text{BiVO}_4:\text{Mo}$ were systematically removed (Supplementary Table 4). The experiments without *S. ovata*. or using heat-killed *S. ovata* cells did not yield any CO_2RR products (Supplementary Tables 3 and 4), thereby confirming that live bacteria are required for the CO_2RR .

A system employing the photocatalyst sheet in a separate compartment from *S. ovata* with the headspace connecting the two chambers (accumulated H_2 concentration of ~6% after 15 h irradiation) produced only ~16% acetate of that obtained from the *S. ovata*|sheet hybrids (Figure 2b). The O_2 evolved accompanied the reduction reactions in a stoichiometric ratio of $(\text{CH}_3\text{COO}^- + \text{H}_2) : \text{O}_2 = 2.1 \pm 0.1$. However, the selectivity of acetate in the obtained products from reduction reactions is only ~7%. This result suggests that growing the bacteria directly at the H_2 evolution site (Figure 3) enables

the biocatalyst to operate under high local H₂ concentrations, avoiding the need for the accumulation of high concentrations of bulk H₂ in the headspace.⁴⁴

CO₂-to-CH₃COO⁻ conversion pathways

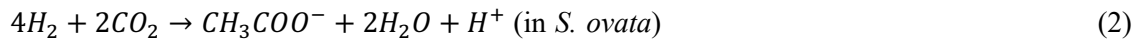
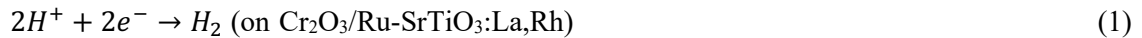
A bacteria-photocatalyst sheet in the absence of the proton reduction cocatalyst Cr₂O₃/Ru on the SrTiO₃:La,Rh surface (Supplementary Table 3) was studied for the artificial photosynthesis reaction. This system also produced CH₃COO⁻ from CO₂ and H₂O (O₂:CH₃COO⁻ = 1.9±0.1) under the same reaction conditions, but the product amounts in 15 h were approximately 80% lower than those observed from the hybrids with Cr₂O₃/Ru loading. The direct utilisation of electrons is consistent with a previous report, where a graphite electrode acted as the electron donor for *S. ovata* to convert CO₂ into CH₃COO⁻.³⁵ Thus, *S. ovata* can use both H₂ and electrons delivered directly to the cells with the photocatalyst sheet for CH₃COO⁻ formation from CO₂ (Figure 1a).

No CH₃COO⁻ was detected in a colloidal system after 15 h irradiation (1 sun), where RuO₂-BiVO₄:Mo powders and *S. ovata* were suspended in the reaction medium. This observation suggests that RuO₂-BiVO₄:Mo could not directly provide *S. ovata* with electrons, possibly due to insufficient driving force from its conduction band (Figure 1a).

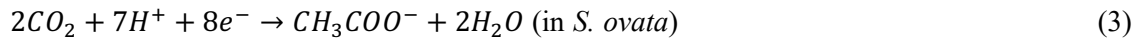
Accordingly, we conclude that CH₃COO⁻ and O₂ are produced by the following mechanism: photoexcitation produces electrons and holes in both SrTiO₃:La,Rh and BiVO₄:Mo when the photocatalyst sheet is exposed to simulated sunlight. The visible light absorption ability of SrTiO₃:La,Rh is due to photoexcitation from the donor levels formed by Rh³⁺ ions to its conduction band.³⁶ In addition, the photoexcited electrons transfer smoothly from BiVO₄:Mo to SrTiO₃:Rh via the ITO nanoparticles.³⁸ Therefore, the photoexcited electrons in BiVO₄:Mo transferred to SrTiO₃:La,Rh and recombined with the holes on the donor levels formed by Rh³⁺ to achieve the Z-scheme photocatalytic reaction. The SrTiO₃:La,Rh is unable to achieve overall water splitting to

produce both H₂ and O₂ (ref. ³³) and the BiVO₄:Mo cannot generate H₂ via proton reduction because its conduction band minimum is more positive than the H⁺ to H₂ reduction potential,⁴⁵ and the H₂ and O₂ production reactions therefore take place on Cr₂O₃/Ru-SrTiO₃:La,Rh and RuO₂-BiVO₄:Mo, respectively, accomplishing via the overall water-splitting reaction. The produced H₂ is taken by *S. ovata* to perform CO₂RR and produces CH₃COO⁻ via the acetyl-CoA Wood-Ljungdahl pathway (Figure 1a). Additionally, *S. ovata* can use photogenerated electrons from illuminated SrTiO₃:La,Rh nanoparticles to perform photosynthesis. The overall photosynthetic pathways are:

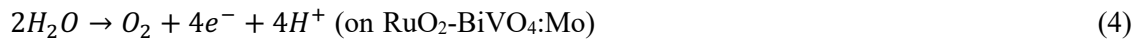
Cathodic reaction:



Or



Anodic reaction:



Overall reaction:



The production of H₂ with Cr₂O₃/Ru-SrTiO₃:La,Rh powder suspended in an aqueous solution containing 18 mM CH₃COO⁻ after 15 h irradiation (pH 8.1; 1 sun) was negligible (< 2 μmol cm⁻²) and the amount of CH₃COO⁻ did not change substantially. Moreover, similar photocurrents for the RuO₂-BiVO₄:Mo|Au photoanode were observed with and without the presence of 18 mM CH₃COO⁻ (Supplementary Fig. 11). Therefore, CH₃COO⁻ was not oxidised by the holes in either SrTiO₃:La,Rh or BiVO₄:Mo in significant amounts, supporting that it does not serve as an electron scavenger in the hybrid system. These observations highlight the clean CO₂-to-CH₃COO⁻ conversion in the current system without substantial limitations from the back reaction with accumulated acetate.

System stability and viability

The CH_3COO^- and O_2 generation rates decreased slowly during the 15 h reaction (Figure 2a). The biological toxicity of each component in the photocatalyst sheet ($\text{Cr}_2\text{O}_3/\text{Ru-SrTiO}_3:\text{La,Rh}$, ITO, $\text{RuO}_2\text{-BiVO}_4:\text{Mo}$) was determined by growing bacteria in presence of individual component powders (Supplementary Fig. 12) and showed that the production of acetate did not change significantly when the bacteria were grown in the presence of $\text{Cr}_2\text{O}_3/\text{Ru-SrTiO}_3:\text{La,Rh}$, ITO or $\text{RuO}_2\text{-BiVO}_4:\text{Mo}$, indicating that these components are not toxic to *S. ovata*. As the gas evolution rates over the bacteria-free $\text{Cr}_2\text{O}_3/\text{Ru-SrTiO}_3:\text{La,Rh}|\text{ITO}|\text{RuO}_2\text{-BiVO}_4:\text{Mo}$ sheet also decreased during water splitting (Supplementary Fig. 7), the drop in activity of the hybrid was assigned to the deactivation of the photocatalyst sheet. The sheet exhibited similar diffuse-reflectance spectra before and after the photosynthetic reaction (Supplementary Fig. 2), indicating an unchanged light absorption of the semiconductors upon the loading of microbes. No notable differences in the phases of $\text{SrTiO}_3:\text{La,Rh}$, $\text{BiVO}_4:\text{Mo}$, and ITO were observed in the X-ray diffraction patterns of the sheet before and after a 15 h water-splitting reaction (Supplementary Fig. 13). The ICP-OES analysis suggested that the Ru amount did not notably change after the water-splitting reaction, but the amount of Cr decreased by ~30% (Supplementary Table 1), demonstrating the partial dissolution of Cr_2O_3 .³⁷

The Cr_2O_3 was then reloaded on the photocatalyst sheet after a 15 h irradiation. The reaction was restarted by inserting the sheet with reloaded Cr_2O_3 and adding the recycled bacteria into a fresh reactant medium purged with 80% N_2 /20% CO_2 (see Methods). The photosynthetic reaction was carried out for 3 runs of 15 h (Figure 4a). The amounts of formed CH_3COO^- and O_2 in the third run were 82% of the initial run even using the recycled bacteria by centrifuging, confirming that bacteria were active within 45 h operation and demonstrating the reusability of the bacterial catalysts. The pH of the reaction medium remained stable (pH 7.2) after each 15-hour photosynthetic reaction. No

obvious changes on the morphologies of photocatalyst sheet were observed after the 45-h reaction, except for the bacteria loading (Supplementary Fig. 14 and 15). The stability for the continuous operation without reloading the Cr₂O₃ could be enhanced by photodepositing TiO₂/CoOOH on the photocatalyst surface to suppress the dissolution of Cr₂O₃ in the cocatalyst.⁴⁶

A high O₂ concentration (> 10%) in the reactor was found to be harmful to *S. ovata*, resulting in in stoichiometric acetate and O₂ production by the *S. ovata*|sheet hybrid. Control experiments show that the CH₃COO⁻ production activity and therefore *S. ovata* growth was not affected by the presence of 4% headspace O₂ (Supplementary Fig. 16). The reactor cell was therefore designed and optimized to ensure that the O₂ concentration did not exceed 4%. The O₂ concentration accumulated in the reactor headspace of the *S. ovata*|sheet hybrid system after 15 h is 3-4%, which is sufficiently low for the bacterium to operate. Activity of strict anaerobes in the presence of O₂ is not unprecedented,⁴⁷ because the presence of enzymes such as superoxide reductase,⁴⁸ superoxide dismutase,⁴⁹ rubredoxins⁵⁰ and NADH⁵¹ oxidase enable protection from O₂ damage. For example, *Geobacter sulfurreducens* (*G. sulfurreducens*), which was previously classified as a strict anaerobe, can survive at low O₂ concentration due to the expression of these oxidative stress enzymes (superoxide dismutase, superoxide reductase, rubredoxins, A-type flavodoxins).⁵² *Desulfovibrio* species can also grow when exposed to O₂ by expressing oxidative stress enzymes,⁵³ and anaerobic homoacetogenic bacteria isolated from terminate guts can reduce O₂ to provide favourable conditions for their growth.⁵⁴ The genome of *S. ovata* also shows the presence of superoxide dismutase, rubredoxins and flavodoxins, which suggests the ability of surviving at least under low O₂ concentrations.⁵⁵ The pH of the reaction medium did not change considerably after 15 h photosynthetic reaction (pH 7.2).

As CO₂ with concentrations of 5-20% is available from coal-fired power plants and many industrial processes,⁵⁶ CO₂ concentration in the purged gas was adjusted from 5 to 20% to investigate its effect on the photosynthetic activity of the *S. ovata*|sheet hybrid system (Figure 4b). The product

generation rates and the selectivity of CH_3COO^- did not dramatically change over this CO_2 concentration range, suggesting that the hybrid system can effectively produce CH_3COO^- from CO_2 with relatively low concentrations.

Power generation from solar-produced acetate

Acetate can be used as a raw material for producing numerous chemicals, including polyvinyl acetate, cellulose acetate, metal acetates, vinyl acetate monomer, volatile organic esters, and alkanes used in making food-grade vinegar, plastics, photographic products, paints, and pharmaceuticals.⁵⁷ Additionally, it can be used as fuel in microbial fuel cells that integrate electroactive bacteria into electrodes for chemical-to-electricity conversion upon demand.^{40,58,59}

To demonstrate accumulation of meaningful quantities and in situ utilisation of acetate from our biohybrid system, we directly used the reaction medium obtained from the 15 h artificial photosynthetic reaction over the *S. ovata*|sheet (contained ~ 9 mM CH_3COO^- ; without removing *S. ovata* cells) as feedstock for a bioelectrochemical anode of a microbial fuel cell (Figure 5a). The bioelectrochemical system consisted of a previously reported porous inverse opal-ITO electrode (IO-ITO, porosity: ~ 10 μm)⁴⁰ inoculated with *G. sulfurreducens* (Supplementary Fig. 17). *G. sulfurreducens* is an electric bacterium that can grow using CH_3COO^- as the electron donor and uses the electrode as the electron acceptor.^{58,59} A control experiment in the absence of acetate demonstrates that *G. sulfurreducens* is incapable of generating current (Supplementary Fig. 18). At a potential of 0.1 V vs. standard hydrogen electrode (SHE), *G. sulfurreducens* started to produce current by metabolizing CH_3COO^- into CO_2 with a maximum current density of 3.08 ± 0.12 mA cm^{-2} and a Faradaic efficiency of $88.2 \pm 6.6\%$ for CH_3COO^- oxidation, which is comparable with the reported benchmark performance (3 mA cm^{-2}) for microbial electrogenesis.⁴⁰ Thus, the CH_3COO^- generated by the *S. ovata*|sheet hybrids can directly serve as a fuel in a microbial fuel cell to produce electricity

upon demand without the removal of *S. ovata* and the extraction and purification of yielded acetate. This demonstration serves as an illustration for a closed carbon cycle, where solar energy is stored by converting CO₂ into acetate and released back to CO₂ when producing renewable electricity.

Conclusions

We have established a strategy to combine the high selectivity of a biological catalyst for clean CO₂-to-C₂ conversion with the light-harvesting and water-splitting ability of semiconductors without the need for organic additives or external bias voltage. The efficient bio-abiotic hybrid prototype (*S. ovata*|Cr₂O₃/Ru-SrTiO₃:La,Rh|ITO|RuO₂-BiVO₄:Mo photocatalyst sheet) produced multi-carbon liquid fuel (CH₃COO⁻) and O₂ in a 1:2 stoichiometric ratio from CO₂ and H₂O using sunlight as the sole energy input, achieving an STA of 0.70 ± 0.04%. The efficient CO₂ fixation over 45 hours and stability benefited from the high viability of *S. ovata*. Additionally, the obtained CH₃COO⁻ can be fed into a biohybrid fuel cell to generate electricity and thereby closes the carbon cycle. The presented bio-abiotic system is comprised of scalable components (photocatalyst sheet and bacteria) and the materials and device preparation is readily accessible and relatively cost-effective without the requirement for vacuum processes. The hybrids operated under ambient conditions (298 K, 1 atm) with relatively low CO₂ concentrations (5-20%), thereby representing a promising strategy towards a practical application of artificial photosynthesis.

The water splitting activity of the present Cr₂O₃/Ru-SrTiO₃:La,Rh|ITO|RuO₂-BiVO₄:Mo photocatalyst sheet is limited by the short absorption edge wavelengths of SrTiO₃:La,Rh and BiVO₄:Mo (~520 nm). The efficiency can be improved by replacing the photocatalyst with narrower bandgap energies. Additionally, genetic engineering would allow for the modification of the electron uptake pathway in acetogenic bacteria in order to increase CO₂ conversion while also redirecting the electron flux to medium-chain fatty acids (e.g., butyric acid) and other higher value products instead

of the natural product acetate.^{7,60} Furthermore, designing a flow reactor can avoid product inhibition to bacteria which can lead to better performance. For example, the current design is compatible with large area photocatalyst sheet reactors (up to 100 m²),⁶¹ where products can be readily extracted from the reaction chamber. The assembly of bacteria on the sheet is straightforward and allows for a large degree of versatility by combining various bacteria and semiconductors to produce a diverse range of solar fuels and chemicals in the future.

Methods

Culturing of *S. ovata*

The strain *S. ovata* was purchased from DSMZ-German Collection of Microorganisms and Cell Cultures GmbH (DSM No.: 2662). *S. ovata* cells were grown using betaine as the electron donor in the DSMZ-recommended growth medium (DSMZ 311) with casitone, Na-resazurin solution, and Na₂S were omitted (Supplementary Table 2). The medium was purged with a mixture of 20%CO₂ and 80%N₂ for 1 hour prior to the inoculation. To investigate the oxygen tolerance of *S. ovata*, the *S. ovata* was grown in a micro-aerobic condition containing 4% O₂ (N₂:CO₂:O₂ = 76:20:4). The inoculated serum vials were kept in a shaking incubator (Incu-Shake MIDI SciQuip; 303 K, 180 rpm) for 6 days. The growth of *S. ovata* was monitored by measuring CH₃COO⁻ concentration (Supplementary Fig. 16) using ¹H NMR (Bruker 400 MHz) and trimethylsilylpropanoic acid (TSP) as the internal standard in D₂O as well as optical density at 600 nm using a UV-Vis spectrometer (Varian Cary 50, Agilent Technologies).

Culturing of *G. sulfurreducens*

G. sulfurreducens PCA (ATCC 51573) was purchased from DSMZ-German Collection of Microorganisms and Cell Cultures GmbH (DSM No.: 12127). *G. sulfurreducens* cells were grown with sodium acetate (20 mM, Sigma-Aldrich, anhydrous, for molecular biology, $\geq 99\%$) as the electron donor and sodium fumarate dibasic (50 mM, Sigma-Aldrich, $\geq 99\%$) as the electron acceptor in the DSMZ-recommended growth medium (DSMZ 826) (Supplementary Table 5). The medium was purged with 20%CO₂/80%N₂ for 1 hour before the inoculation. The inoculated serum vials were kept in a shaking incubator (303 K, 180 rpm) for 6 days. The concentration of bacterial suspension was determined by measuring optical density at 600 nm using the UV-vis spectrometer.

Preparation of SrTiO₃:La,Rh|ITO|BiVO₄:Mo photocatalyst sheets

A two-step solid-state reaction was used to synthesise SrTiO₃:La,Rh (La/(La + Sr) = Rh/(Rh + Ti) = 4 mol%) according to a previously reported procedure.¹⁹ SrCO₃ (Alfa Aesar, 99.99%) and rutile TiO₂ (Sigma-Aldrich, $\geq 99.98\%$) powders (Sr/Ti = 1.05) were mixed in a mortar, followed by calcination in an alumina crucible at 1473 K for 10 h. Subsequently, La₂O₃ (Fisher Scientific, 99.99%) and Rh₂O₃ (Wako Pure Chemical, 98.0–102.0%) were added into the resulting SrTiO₃ and heated at 1373 K for 6 h.

BiVO₄:Mo (Mo/V = 0.05 mol%) was synthesised through aqueous processes.¹⁹ A layered Mo-doped K₃V₅O₁₄ was first obtained by calcining the mixture of K₂CO₃ (Breckland Scientific, 99.5%), V₂O₅ (Fisher Scientific, 99.6%), and MoO₃ (Mo/V = 0.05 mol%, BDH Chemicals, 99.5%) in air at 723 K for 5 h. Stoichiometric Bi(NO₃)₃·5H₂O (Sigma-Aldrich, 98%) was added to 100 mL distilled water to form a suspension of BiONO₃. The resulting Mo-doped K₃V₅O₁₄ was added to the BiONO₃ suspension and stirred mildly at 343 K for 10 h. The obtained powder was collected by filtration, washed with distilled water, and then dried overnight in air before use.

SrTiO₃:La,Rh|ITO|BiVO₄:Mo photocatalyst sheets were prepared by a drop-casting method. A mixture of SrTiO₃:La,Rh, BiVO₄:Mo powders (2.5 mg each), and ITO nanoparticles (Sigma-Aldrich, average size 30 nm; 1.2 mg) was suspended in isopropanol (Sigma-Aldrich, ≥99.5%, 0.25 mL) by ultrasonication for 30 min and then drop-cast on a glass substrate (ca. 1.5 cm × 1.5 cm). The obtained sheet was dried in air at room temperature. The SrTiO₃:La,Rh|ITO|BiVO₄:Mo sheet was obtained after annealing in air at 573 K for 30 min.

Cocatalyst loading on the photocatalyst sheet

The photocatalyst sheets were modified with nanoparticulate Ru species by photodeposition.¹⁹ The photodeposition reactions were conducted in a closed system with side illumination from a 150 W Xe lamp (Newport Oriel 6255; $\lambda > 200$ nm) with an infrared water filter. The photocatalyst sheet samples (~2.2 cm²) were attached to a steel rod and inserted into the reaction cell. In the initial step, Ru species were photodeposited on the photocatalyst sheets from RuCl₃ (Acros Organics, 35–40% ruthenium) dissolved in distilled water (35 ml). Subsequently, the reactant was changed to an aqueous K₂CrO₄ solution (Sigma-Aldrich, ≥99 %) and a thin Cr₂O₃ layer was coated on metallic Ru nanoparticles on the surface of SrTiO₃:La,Rh by photodeposition.^{19,39} The amounts of RuCl₃ and K₂CrO₄ were 0.3 and 0.15 μmol for a photocatalyst sheet sample 2.2 cm² in size. Before performing the photodeposition reaction, the reactant in the cell was purged for 30 min with N₂ containing 2% CH₄ as an internal standard for gas chromatography measurements. The pH of the reactant after N₂ purging was 6.9. The photodeposition was monitored by measuring produced amounts of H₂ and O₂. The photodeposition was finished when the gas evolution rates became steady, typically 10 and 6 hours for Ru and Cr₂O₃ deposition, respectively.

For the experiments without loading of Cr₂O₃/Ru as H₂ evolution cocatalyst on the photocatalyst sheet, RuO₂ (1 wt%) was loaded on BiVO₄:Mo particles in advance of the sheet preparation by an

impregnation method.³² BiVO₄:Mo powder (0.1–0.2 g) was put in an evaporating dish. After adding an aqueous solution containing a given amount of RuCl₃, the evaporating dish was placed in a water bath. The powder was collected and calcined in air at 623 K for 1 h when the solution was evaporated to dryness.

Fabrication of photoelectrodes

The IO-ITO electrode was prepared by a previously reported co-assembly method.⁴⁰ Initially, ITO nanoparticles (Sigma-Aldrich, average size < 50 nm; 20 mg) were added into a mixture of methanol and water (11:1 v:v; 125 μ L) and sonicated for 3 h. Polystyrene (PS) latex (Polysciences Inc.; 10 μ m, 0.75 mL, 2.5 wt% in water) was centrifuged at 10,000 rpm for 3 min to remove the supernatant. The ITO nanoparticles dispersion was mixed with the PS beads and sonicated for 30 min in ice water (< 277 K) to obtain a uniform mixture. The PS-ITO mixture (15 μ L) was drop-casted onto an ITO glass slide (Visiontek System Ltd.; 1 cm \times 2.5 cm \times 0.11 cm, 12 Ω cm⁻²) with a pre-defined area of 0.25 cm², and kept drying in air for 30 min. The IO-ITO electrodes were obtained by annealing the glass slides at 773 K in air for 20 min at a ramping rate of 1 K min⁻¹ from room temperature. The thickness of the IO-ITO scaffold was \sim 60 μ m (Supplementary Fig. 17b). Copper wires were embedded in indium at the bottom of the sample to establish electrical contact. The copper wire and indium were encapsulated with epoxy (Araldite, Rapid 5-Minute Epoxy).

Characterisation

The diffuse-reflectance spectra were obtained using an ultraviolet-visible-near-infrared spectrometer (Varian Cary 50 Bio). A TESCAN MIRA3 FEG-SEM instrument with an Oxford Instruments Aztec Energy X-maxN 80 system was used to collect the SEM and SEM-EDX element mapping images at an acceleration voltage of 5 and 15 kV, respectively. X-ray diffraction patterns of

the samples were measured with a PANalytical Empyrean Series 2 instrument using Cu K α source operated at 40 kV and 40 mA. ICP-OES measurements were carried out on a Thermo Scientific iCAP 7400 ICP-OES DUO spectrometer. Analyte solutions for ICP-OES were obtained by digesting the sheets in aqueous HNO₃ (>68%) for one day and dilution to 2% vol/vol with Milli-Q water.

Protein quantification

The protein concentrations were quantified with the Bio-Rad protein assay (Bio-Rad Protein Assay Kit #5000002) as previously reported.⁶² Bacteria attached on the photocatalyst sheet were dipped in a sodium dodecyl solution (5 mL, 10 wt%) solution at 372 K for 15 min to extract proteins from the sample. The solution was centrifuged (14,000 rpm, 10 min) to remove the impurities. The supernatant was then collected to quantify the protein by the Bio-Rad protein assay utilising the principle of protein-dye binding. 5 mL of the diluted dye reagent, which was incubated at 298 K for 10 min, was added in a clean vial containing the protein solution (100 μ L). The absorbance of the solution at 600 nm was measured using the UV-vis spectrometer. Bovine serum albumin was used as the protein standard to make the correlation curve and the protein concentration was calculated from the standard curve.

Photocatalytic reactions

The photocatalytic reactions were performed in a closed system with side illumination from Newport Oriel 67005 solar light simulators (150 W, 100 mW cm⁻² across the solar spectrum, AM 1.5 G, $\lambda > 200$ nm) with infrared water filter, which were calibrated using a certified Newport 1916-R optical power meter. The photocatalyst sheet samples (ca. 2.2 cm²) were attached to a steel rod and inserted into the reaction cell containing an *S. ovata* medium (DSMZ 311) without betaine, Naresazurin solution, casitone, L-cysteine, yeast extract, and Na₂S (Supplementary Table 2) (12 mL)

unless otherwise noted. Before conducting the CO₂RR, the reactant in the cell was purged for 40 min with the mixture of N₂ and CO₂ (N₂:CO₂ = 80:20), unless otherwise noted. The betaine-grown *S. ovata* cells were then injected into the reactor (final optical density at 600 nm: 0.6) and purged with the same gas mixture for another 20 minutes. The pH of the medium after purging was 7.0.

The sheet and bacteria separated system (Figure 2b) employed the photocatalyst sheet in a separate compartment from *S. ovata* with the headspace connecting the two chambers. The two chambers contained the same reaction medium purged with the mixture of N₂ and CO₂ (N₂:CO₂ = 80:20), as mentioned above.

In the 45-h photosynthetic reaction, Cr₂O₃ was reloaded every 15 h. The photocatalyst sheet was taken out of the reaction medium after the first run and put in a fresh reaction medium added with 0.15 μmol K₂CrO₄. The photodeposition was carried out for 3 h under a 150 W Xe lamp irradiation. The photocatalyst sheet was then inserted in another new reaction medium to start the second run. The reactant was purged for 40 min with the mixture of N₂ and CO₂ (N₂:CO₂ = 80:20). The *S. ovata* cells obtained from the reaction medium in the first run by centrifugation were then injected into the reactor and purged with the same gas mixture for another 20 minutes. Subsequently, the reaction was restarted by exposing to the simulated sunlight illumination (AM 1.5G, 100 mW cm⁻²).

The water-splitting reaction using the Cr₂O₃/Ru-SrTiO₃:La,Rh|ITO|RuO₂-BiVO₄:Mo photocatalyst sheet in the absence of *S. ovata* was carried out in the same reaction medium purging with N₂ containing 2% CH₄ as an internal standard for gas chromatography measurements.

In the colloidal systems for photocatalytic CO₂RR over *S. ovata*|RuO₂-BiVO₄:Mo, RuO₂-BiVO₄:Mo powder (2 mg) was dispersed in an *S. ovata* medium (2 mL) in Pyrex glass photoreactor vials capped with rubber septa. The samples were purged with a mixture of N₂ and CO₂ (N₂:CO₂ = 80:20) for 40 min. After injecting the betaine-grown *S. ovata* cells, the reactor was purged with the same gas mixture for another 20 min. For the H₂ evolution reaction over SrTiO₃:La,Rh in the presence

of CH_3COO^- , $\text{SrTiO}_3:\text{La,Rh}$ powder (2 mg) was added to an aqueous solution of CH_3COONa (18 mM, 2 mL). After briefly vortexing, the samples were purged with N_2 containing 2% CH_4 as an internal standard at ambient pressure for 40 min. The above reactions were carried out under simulated sunlight irradiation (AM 1.5G, 100 mW cm^{-2}).

Products quantification

Concentrations of CH_3COO^- were measured by ^1H NMR spectroscopy (Bruker 400 MHz) with trimethylsilylpropanoic acid (TSP) as the internal standard in D_2O . Spectra were processed using the Bruker TopSpin Software. A Shimadzu GC-2010 Plus gas chromatograph equipped with a barrier discharge ionisation detector was used to quantify H_2 . The GC-2010 Plus was equipped with Hayesep D (2 m * 1/8'' OD * 2 mm ID, 80/100 mesh, Analytical Columns) pre-column and a RT-Molsieve 5A (30 m * 0.53 mm ID, Restek) main column. Aliquots (50 μL) of the headspace gas were collected from the sealed cell using a gastight syringe (Hamilton, GASTIGHT 1710) for gas chromatography analysis. The O_2 quantification was performed in a glovebox (O_2 concentration < 3 ppm) using a NeoFox-GT fluorometer and Fospor-R fluorescence oxygen sensor probe from Ocean Optics. The analytical errors are <5% for quantifying H_2 and <10% for O_2 .

Isotopic labelling

The photosynthetic reaction over $S. ovata|\text{Cr}_2\text{O}_3/\text{Ru-SrTiO}_3:\text{La,Rh}|\text{ITO}|\text{RuO}_2\text{-BiVO}_4:\text{Mo}$ hybrid system was performed in a reaction medium containing 47 mM $\text{NaH}^{13}\text{CO}_3$ (Sigma-Aldrich, 98 atom% ^{13}C , 99% (CP)) with the mixture of N_2 and $^{13}\text{CO}_2$ (Sigma-Aldrich, 99.0 atom % ^{13}C , 99% (CP); $\text{N}_2:^{13}\text{CO}_2 = 80:20$) as the headspace gas. The amounts of CH_3COO^- produced in 5 and 15 h were analysed by ^1H NMR and ^{13}C NMR spectroscopy conducted on a Bruker 400 MHz spectrometer.

Quantum yield measurements

The AQY of the photosynthetic reaction was calculated using

$$\text{AQY} = (16R/I) \times 100\% \quad (6)$$

Where R and I denote the CH_3COO^- production rate and the photon flux of monochromatic light, respectively. To form one acetate molecule, eight electrons in $\text{SrTiO}_3:\text{La},\text{Rh}$ must be consumed in the CO_2RR . Meanwhile, eight electrons in $\text{BiVO}_4:\text{Mo}$ must be combined with the holes in $\text{SrTiO}_3:\text{La},\text{Rh}$. Sixteen electrons are therefore required to produce one acetate molecule. The AQYs were determined using a LOT MSH-300 monochromator. Thorlabs PM100D power meter and Thorlabs S302C thermal power sensor were used to measure power at different wavelengths. The wavelength λ with a full width at half maximum of 15 nm was varied between 390 and 540 nm in 30 nm steps.

Solar-to-acetate (STA) conversion efficiency

The STA is given as

$$\text{STA} (\%) = (R(\text{CH}_3\text{COO}^-) \times \Delta G_r) / (P \times S) \times 100 \quad (7)$$

where $R(\text{CH}_3\text{COO}^-)$, ΔG_r , P , and S indicate the rate of CH_3COO^- formation during the photosynthetic reaction, the energy intensity of the AM 1.5G solar irradiation (100 mW cm^{-2}) and the irradiated sample area, respectively.

Microbial electrogenesis

The CH_3COO^- (~9 mM; 15 mL) produced by *S. ovata*| $\text{Cr}_2\text{O}_3/\text{Ru}-\text{SrTiO}_3:\text{La},\text{Rh}$ |ITO| $\text{RuO}_2-\text{BiVO}_4:\text{Mo}$ hybrid system via a 15 h photosynthetic reaction was used as feedstock and electrolyte to generate electricity using *G. sulfurreducens* as the model electric bacterium. The microbial electrogenesis on *G. sulfurreducens*|IO-ITO electrode (0.25 cm^2) was performed in a three-electrode configuration using a Ag/AgCl reference electrode (in saturated NaCl aqueous solution, Basi MW-

2030) and a platinum mesh counter electrode. The solution obtained from the photosynthetic reaction was purged with a mixture of N₂ and CO₂ (N₂:CO₂ = 80:20) for 40 minutes. The freshly grown *G. sulfurreducens* was inoculated into the reactor (final optical density at 600 nm: 0.6) and purged for another 20 minutes. The reactor was kept at constant temperature (303 K) and stirring (200 rpm). The working electrode was poised with a potential of 0.1 V vs SHE using a potentiostat (MultiEmStat3+).

Statistics and Reproducibility

The mean values and standard deviations of data sets are calculated using the AVERAGE and STDEV.S function of Microsoft Excel (Microsoft 365), respectively. Regarding the SEM and SEM-EDX element mapping images, two to five distinct locations with similar morphologies were captured for each sample and representative images are shown.

Data availability

All source data that support the findings of this study are available from the University of Cambridge data repository: <https://doi.org/10.17863/CAM.84871>.

Acknowledgements

We thank Dr Motiar Rahaman, Dr Lin Su, and Miss Melanie Miller (University of Cambridge) for helpful discussions and Dr Heather Greer at the University of Cambridge for assisting in the collection of SEM-EDX element mapping images. This work was supported by a European Research Council (ERC) Consolidator Grant ‘MatEnSAP’ (682833 to E.R.), UK Research and Innovation Cambridge Creative Circular Plastics Centre (grant EP/S025308), European Marie Skłodowska-Curie individual Fellowships (to Q.W., GAN 793996 and to S.K., GAN 744317), Research England’s Expanding

Excellence in England (E3) Fund (to S.K.), the Cambridge Trust (Cambridge Thai Foundation Award to C.P.) and a Trinity-Henry Barlow Scholarship (to C.P.).

Author contributions

Q.W., S.K., and E.R. conceived the idea and designed the project. Q.W. prepared the photocatalyst sheet and photoelectrodes and conducted physical characterisations of the semiconductors. S.K. and Q.W. carried out the bacteria culturing. S.K. quantified the protein and performed the microbial electrogenesis. C.P. recorded the SEM and SEM-EDX element mapping images. Q.W. and C.P. carried out H₂ and O₂ qualification. S.K., C.D.S., and C.P. quantified acetate. The O₂-tolerance ability of bacteria was investigated by C.D.S. and S.K. C.D.S., S.K., and Q.W. conducted the isotopic labelling experiments. All authors analysed the data and discussed the results. Q.W., S.K., and E.R. wrote the manuscript with assistance from the other co-authors. E.R. supervised the project.

Competing interests

The authors declare no competing interests.

Figure 1 | *S. ovata*|sheet hybrid system. a, Mechanistic pathway diagram depicting the photosynthetic CO₂-to-acetate conversion coupled with water oxidation over *S. ovata*|Cr₂O₃/Ru-SrTiO₃:La,Rh|ITO|RuO₂-BiVO₄:Mo. CB and VB indicate conduction band and valence band, respectively. M_{ox} and M_{red} represent intracellular oxidized and reduced redox mediators, respectively. *hν* indicates light irradiation. The conduction and valence band potentials for SrTiO₃:La,Rh are located at -0.9 and +2.3 V vs. NHE at pH 7, respectively.³⁶ The visible light absorption ability of SrTiO₃:La,Rh is assigned to photoexcitation from the donor levels formed by Rh³⁺ ions (+1.7 vs. NHE at pH 7) to its conduction band. BiVO₄:Mo has a conduction band and valence band potential

of -0.3 and $+2.1$ V vs. NHE at pH 7, respectively.⁴⁵ The reduction potential of H^+/H_2 and O_2/H_2O is -0.41 and $+0.82$ V (vs. NHE at pH 7), respectively. The reduction potential of CO_2/CH_3COO^- (-0.3 vs. NHE at pH 7) was determined by the reaction Gibbs energy of the CO_2 -to- CH_3COO^- conversion coupled with water oxidation (873 kJ mol⁻¹ at 1 atm and 298 K).¹⁴ **b-c**, Photographs of 1.5 cm \times 1.5 cm $Cr_2O_3/Ru-SrTiO_3:La,Rh|ITO|RuO_2-BiVO_4:Mo$ photocatalyst sheets before (**b**) and after (**c**) 15 h photosynthetic reaction.

Figure 2 | Photosynthetic activity of the *S. ovata*/sheet hybrids. **a**, Time course of the photosynthetic CH_3COO^- , O_2 and H_2 production over $S. ovata|Cr_2O_3/Ru-SrTiO_3:La,Rh|ITO|RuO_2-BiVO_4:Mo$ hybrids. Error bars correspond to the standard deviation ($n = 3$ independent samples). The open circles and solid circles indicate the individual data points and mean values, respectively. The light blue area represents the standard deviation for O_2 evolution. The red and purple vertical lines represent the standard deviation for CH_3COO^- and H_2 , respectively. The dashed lines are guides to the eye. **b**, Time course of the CH_3COO^- , O_2 and H_2 production over a system separated the photocatalyst sheet and *S. ovata* into two chambers. Error bars correspond to the standard deviation ($n = 2$ independent samples). The open circles and solid circles indicate the individual data points and mean values, respectively. The light blue area represents the standard deviation for O_2 evolution. The red and purple vertical lines represent the standard deviation for CH_3COO^- and H_2 , respectively. The dashed lines are guides to the eye. **c**, Dependence of AQY for CH_3COO^- production on incident light wavelength, along with diffuse reflectance spectra of $SrTiO_3:La,Rh$ (red dashed line), and $BiVO_4:Mo$ (red line) for comparison. The blue dots indicate the AQYs of the system at various incident light wavelengths. The full width at half maximum of incident wavelength is 15 nm. F(R), Kubelka–Munk function. **d**, 1H NMR spectra (D_2O , 400 MHz) of the solution after 5 and 15 h of irradiation using $^{12}CO_2/H^{12}CO_3^-$ (yellow and orange trace, respectively) and $^{13}CO_2/H^{13}CO_3^-$ (light green and dark green

trace, respectively) as the carbon sources. The reactions were carried out in a reaction medium purged with 80%N₂:20%CO₂ (pH 7.0) under ambient conditions (298 K, 1 atm) and 1 sun illumination (AM 1.5G, 100 mW cm⁻²).

Figure 3 | Morphology of *S. ovata*|sheet hybrids. **a**, Top-view SEM image of a *S. ovata*|Cr₂O₃/Ru-SrTiO₃:La,Rh|ITO|RuO₂-BiVO₄:Mo sheet after 15 h photosynthetic reaction over the hybrid system. **b-e**, Top-view SEM-EDX elemental mapping images of a *S. ovata*|Cr₂O₃/Ru-SrTiO₃:La,Rh|ITO|RuO₂-BiVO₄:Mo sheet after 15 h photosynthetic reaction over the hybrid system, showing a superimposition (**b**) of the distributions of Sr (**c**), Bi (**d**) and In (**e**).

Figure 4 | Viability of the *S. ovata*|sheet hybrids. **a**, Products accumulation for 3 runs of 15 hours, with the reloading of Cr₂O₃ on the *S. ovata*|Cr₂O₃/Ru-SrTiO₃:La,Rh|ITO|RuO₂-BiVO₄:Mo hybrid and replenishing the reactant medium with a fresh solution and 80%N₂/20%CO₂ purging every 15 hours. The sample areas were ~2.2 cm². Error bars correspond to the standard deviation (n = 3 independent samples). The bars show the mean values and the black vertical lines indicate the standard deviation. The open circles represent the individual data points. **b**, Dependence of the photosynthetic activity of the *S. ovata*|Cr₂O₃/Ru-SrTiO₃:La,Rh|ITO|RuO₂-BiVO₄:Mo hybrid system on the CO₂ concentration in the headspace. Error bars correspond to the standard deviation (n = 2 independent samples). The bars show the mean values and the black vertical lines indicate the standard deviation. The open circles represent the individual data points. The reactions were carried out in a reaction medium purged with 80%N₂:20%CO₂ (pH 7.0) under ambient conditions (298 K, 1 atm) and 1 sun illumination (AM 1.5G, 100 mW cm⁻²).

Figure 5 | *G. sulfurreducens*|IO-ITO electrode producing electricity. **a**, Schematic diagram showing that the sunlight-driven *S. ovata*|Cr₂O₃/Ru-SrTiO₃:La,Rh|ITO|RuO₂-BiVO₄:Mo hybrid provides a biohybrid electrochemical system with CH₃COO⁻ to realise the current generation and close the carbon cycle. IO-ITO represents porous inverse opal-ITO electrode. **b**, Current production by *G. sulfurreducens*|IO-ITO electrode at 0.1 V vs. SHE with CH₃COO⁻ (ca. 9 mM; pH 7.2, 303 K), which was produced in 15 h by the *S. ovata*|Cr₂O₃/Ru-SrTiO₃:La,Rh|ITO|RuO₂-BiVO₄:Mo hybrid system under simulated sunlight irradiation (AM 1.5G, 100 mW cm⁻²). Error bars correspond to the standard deviation (n = 3 independent samples). The red circles indicate the mean values and the light red area represents the standard deviation.

References

1. Jiang, K. *et al.* Metal ion cycling of Cu foil for selective C–C coupling in electrochemical CO₂ reduction. *Nat. Catal.* **1**, 111–119 (2018).
2. Morales-Guio, C. G. *et al.* Improved CO₂ reduction activity towards C₂₊ alcohols on a tandem gold on copper electrocatalyst. *Nat. Catal.* **1**, 764–771 (2018).
3. Nitopi, S. *et al.* Progress and perspectives of electrochemical CO₂ reduction on copper in aqueous electrolyte. *Chem. Rev.* **119**, 7610–7672 (2019).
4. García de Arquer, F. P. *et al.* CO₂ electrolysis to multicarbon products at activities greater than 1 A cm⁻². *Science* **367**, 661–666 (2020).
5. Rahaman, M., Dutta, A., Zanetti, A. & Broekmann, P. Electrochemical reduction of CO₂ into multicarbon alcohols on activated Cu mesh catalysts: an identical location (IL) study. *ACS Catal.* **7**, 7946–7956 (2017).

6. Birdja, Y. Y. *et al.* Advances and challenges in understanding the electrocatalytic conversion of carbon dioxide to fuels. *Nat. Energy* **4**, 732–745 (2019).
7. Claassens, N. J., Sousa, D. Z., dos Santos, V. A. P. M., de Vos, W. M. & van der Oost, J. Harnessing the power of microbial autotrophy. *Nat. Rev. Microbiol.* **14**, 692–706, (2016).
8. Lapinsonnière, L., Picot, M. & Barrière, F. Enzymatic versus microbial bio-catalyzed electrodes in bio-electrochemical systems. *ChemSusChem* **5**, 995–1005 (2012).
9. Cestellos-Blanco, S., Zhang, H., Kim, J. M., Shen, Y.-x. & Yang, P. Photosynthetic semiconductor biohybrids for solar-driven biocatalysis. *Nat. Catal.* **3**, 245–255 (2020).
10. Kornienko, N., Zhang, J. Z., Sakimoto, K. K., Yang, P. & Reisner, E. Interfacing nature's catalytic machinery with synthetic materials for semi-artificial photosynthesis. *Nat. Nanotechnol.* **13**, 890–899 (2018).
11. Bian, B., Bajracharya, S., Xu, J., Pant, D. & Saikaly, P. E. Microbial electrosynthesis from CO₂: Challenges, opportunities and perspectives in the context of circular bioeconomy. *Bioresour. Technol.* **302**, 122863 (2020).
12. Li, H. *et al.* Integrated electromicrobial conversion of CO₂ to higher alcohols. *Science* **335**, 1596–1596 (2012).
13. Haas, T., Krause, R., Weber, R., Demler, M. & Schmid, G. Technical photosynthesis involving CO₂ electrolysis and fermentation. *Nat. Catal.* **1**, 32–39 (2018).
14. Liu, C. *et al.* Nanowire–Bacteria hybrids for unassisted solar carbon dioxide fixation to value-added chemicals. *Nano Lett.* **15**, 3634–3639 (2015).
15. Nichols, E. M. *et al.* Hybrid bioinorganic approach to solar-to-chemical conversion. *Proc. Natl. Acad. Sci. U. S. A.* **112**, 11461–11466 (2015).

16. Liu, C., Colón, B. C., Ziesack, M., Silver, P. A. & Nocera, D. G. Water splitting–biosynthetic system with CO₂ reduction efficiencies exceeding photosynthesis. *Science* **352**, 1210–1213 (2016).
17. Sakimoto, K. K., Zhang, S. J. & Yang, P. Cysteine–cystine photoregeneration for oxygenic photosynthesis of acetic acid from CO₂ by a tandem inorganic–biological hybrid system. *Nano Lett.* **16**, 5883–5887 (2016).
18. Su, Y. *et al.* Close-packed nanowire-bacteria hybrids for efficient solar-driven CO₂ fixation. *Joule*, **4**, 800–811 (2020).
19. Wang, Q. *et al.* Scalable water splitting on particulate photocatalyst sheets with a solar-to-hydrogen energy conversion efficiency exceeding 1%. *Nat. Mater.* **15**, 611–615 (2016).
20. Geisz, J. F. *et al.* Six-junction III–V solar cells with 47.1% conversion efficiency under 143 Suns concentration. *Nat. Energy* **5**, 326–335 (2020).
21. Yoshikawa, K. *et al.* Silicon heterojunction solar cell with interdigitated back contacts for a photoconversion efficiency over 26%. *Nat. Energy* **2**, 17032 (2017).
22. Ager, J. W., Shaner, M. R., Walczak, K. A., Sharp, I. D. & Ardo, S. Experimental demonstrations of spontaneous, solar-driven photoelectrochemical water splitting. *Energy Environ. Sci.* **8**, 2811–2824 (2015).
23. Ardo, S. *et al.* Technical and economic feasibility of centralized facilities for solar hydrogen production via photocatalysis and photoelectrochemistry. *Energy Environ. Sci.* **6**, 1983–2002 (2013).
24. Pinaud, B. A. *et al.* Technical and economic feasibility of centralized facilities for solar hydrogen production via photocatalysis and photoelectrochemistry. *Energy Environ. Sci.* **6**, 1983–2002 (2013).

25. Gai, P. *et al.* Solar-powered organic semiconductor–bacteria biohybrids for CO₂ reduction into acetic acid. *Angew. Chem. Int. Ed.* **59**, 7224–7229 (2020).
26. Sakimoto, K. K., Wong, A. B. & Yang, P. Self-photosensitization of nonphotosynthetic bacteria for solar-to-chemical production. *Science* **351**, 74–77 (2016).
27. Zhang, H. *et al.* Bacteria photosensitized by intracellular gold nanoclusters for solar fuel production. *Nat. Nanotechnol.* **13**, 900–905 (2018).
28. Göbbels, L. *et al.* Cysteine: an overlooked energy and carbon source. *Sci. Rep.* **11**, 2139 (2021).
29. Kaden, J., S. Galushko, A. & Schink, B. Cysteine-mediated electron transfer in syntrophic acetate oxidation by cocultures of *Geobacter sulfurreducens* and *Wolinella succinogenes*. *Arch. Microbiol.* **178**, 53–58 (2002).
30. Liu, D., Dong, H., Zhao, L. & Wang, H. Smectite reduction by *Shewanella* species as facilitated by cystine and cysteine. *Geomicrobiol. J.* **31**, 53–63 (2014).
31. Zhu, S. & Wang, D. Photocatalysis: Basic principles, diverse forms of implementations and emerging scientific opportunities. *Adv. Energy Mater.* **7**, 1700841 (2017).
32. Wang, Q. *et al.* Molecularly engineered photocatalyst sheet for scalable solar formate production from carbon dioxide and water. *Nat. Energy*, **5**, 703–710 (2020).
33. Wang, Q. *et al.* Z-scheme water splitting using particulate semiconductors immobilized onto metal layers for efficient electron relay. *J. Catal.* **328**, 308–315 (2015).
34. Li, X., Yu, J. Jaroniec, M. & Chen, X. Cocatalysts for selective photoreduction of CO₂ into solar fuels. *Chem. Rev.* **119**, 3962–4179 (2019).
35. Nevin, K. P., Woodard, T. L., Franks, A. E., Summers, Z. M. & Lovley, D. R. Microbial electrosynthesis: feeding microbes electricity to convert carbon dioxide and water to multicarbon extracellular organic compounds. *mBio* **1**, e00103–00110 (2010).

36. Moss, B. *et al.* Linking in situ charge accumulation to electronic structure in doped SrTiO₃ reveals design principles for hydrogen-evolving photocatalysts. *Nat. Mater.* **20**, 511–517 (2021).
37. Wang, Q. *et al.* Printable photocatalyst sheets incorporating a transparent conductive mediator for Z-scheme water splitting. *Joule* **2**, 2667–2680 (2018).
38. Ebihara, M. *et al.* Charge carrier mapping for Z-scheme photocatalytic water-splitting sheet via categorization of microscopic time-resolved image sequences. *Nat. Commun.* **12**, 3716 (2021).
39. Maeda, K. *et al.* Noble-Metal/Cr₂O₃ core/shell nanoparticles as a cocatalyst for photocatalytic overall water splitting. *Angew. Chem. Int. Ed.* **45**, 7806–7809 (2006).
40. Fang, X., Kalathil, S., Divitini, G., Wang, Q. & Reisner, E. A three-dimensional hybrid electrode with electroactive microbes for efficient electrogenesis and chemical synthesis. *Proc. Natl. Acad. Sci. U. S. A.* **117**, 5074–5080 (2020).
41. Cerdan, S., Künnecke, B. & Seelig, J. Cerebral metabolism of [1,2-¹³C₂]acetate as detected by in vivo and in vitro ¹³C NMR. *J. Biol Chem.* **265**, 12916–12926 (1990).
42. Wasylenko, T. M. & Stephanopoulos, G. Kinetic isotope effects significantly influence intracellular metabolite ¹³C labeling patterns and flux determination. *Biotechnol. J.* **8**, 1080–1089 (2013).
43. Millard, P., Portais, J.-C. & Mendes, P. Impact of kinetic isotope effects in isotopic studies of metabolic systems. *BMC Syst. Biol.* **9**, 1–13 (2015).
44. Morello, G., Megarity, C. F. & Armstrong, F. A. The power of electrified nanoconfinement for energising, controlling and observing long enzyme cascades. *Nat. Commun.* **12**, 340 (2021).
45. Kudo, A., Omori, K. & Kato, A novel aqueous process for preparation of crystal form-controlled and highly crystalline BiVO₄ powder from layered vanadates at room temperature and its photocatalytic and photophysical properties. *J. Am. Chem. Soc.* **121**, 11459–11467 (1999).

46. Lyu, H. *et al.* An Al-doped SrTiO₃ photocatalyst maintaining sunlight-driven overall water splitting activity for over 1000 h of constant illumination. *Chem. Sci.* **10**, 3196–3201 (2019).
47. Lu, Z. & Imlay, J. A. When anaerobes encounter oxygen: mechanisms of oxygen toxicity, tolerance and defence. *Nat. Rev. Microbiol.* **19**, 774–785 (2021).
48. Jenney, F. E., Verhagen, M. F. J. M., Cui, X. & Adams, M. W. W. Anaerobic microbes: oxygen detoxification without superoxide dismutase. *Science* **286**, 306–309 (1999).
49. Nakanishi, T., Inoue, H. & Kitamura, M. Cloning and expression of the superoxide dismutase gene from the obligate anaerobic bacterium *Desulfovibrio vulgaris* (Miyazaki F). *J. Biochem.* **133**, 387–393 (2003).
50. Lumpio, H. L., Shenvi, N. V., Summers, A. O., Voordouw, G. & Kurtz, D. M. Rubrerythrin and rubredoxin oxidoreductase in *Desulfovibrio vulgaris*: a novel oxidative stress protection system. *J. Bacteriol.* **183**, 101–108 (2001).
51. Ward, D. E. *et al.* The NADH oxidase from *Pyrococcus furiosus*. *Eur. J. Biochem.* **268**, 5816–5823 (2001).
52. Lin, W. C., Coppi, M. V. & Lovley, D. R. *Geobacter sulfurreducens* can grow with oxygen as a terminal electron acceptor. *Appl. Environ. Microbiol.* **70**, 2525–2528 (2004).
53. Abdollahi, H. & Wimpenny, J. W. T. Effects of oxygen on the growth of *Desulfovibrio desulfuricans*. *Microbiology* **136**, 1025–1030 (1990).
54. Boga, H. I., Brune, A. Hydrogen-dependent oxygen reduction by homoacetogenic bacteria isolated from termite guts. *Appl. Environ. Microbiol.* **69**, 779–786 (2003).
55. Poehlein, A., Gottschalk, G. & Daniel, R. First insights into the genome of the gram-negative, endospore-forming organism *Sporomusa ovata* strain H1 DSM 2662. *Genome. Announc.* **1**, e00734–00713 (2013).

56. Last, G. V. & Schmick, M. T. A review of major non-power-related carbon dioxide stream compositions. *Environ. Earth Sci.* **74**, 1189–1198 (2015).
57. Agreda, V. H. *Acetic Acid and Its Derivatives Chemical Industries*. (CRS Press, New York, 1992).
58. Bond, D. R. & Lovley, D. R. Electricity production by *Geobacter sulfurreducens* attached to electrodes. *Appl. Environ. Microbiol.* **69**, 1548–1555 (2003).
59. Logan, B. E., Rossi, R., Ragab, A. a. & Saikaly, P. E. Electroactive microorganisms in bioelectrochemical systems. *Nat. Rev. Microbiol.* **17**, 307–319 (2019).
60. Clomburg, J. M., Crumbley, A. M. & Gonzalez, R. Industrial biomanufacturing: The future of chemical production. *Science* **355**, 38 (2017).
61. Nishiyama, H. *et al.* Photocatalytic solar hydrogen production from water on a 100 m²-scale. *Nature* **598**, 304–307 (2021).
62. Bradford, M. M. A rapid and sensitive method for the quantitation of microgram quantities of protein utilizing the principle of protein-dye binding. *Anal. Biochem.* **72**, 248–254 (1976).